Wave Breaking on a Sloping Beach: Comparison Between Experiments and Simulations

Alexei Goumilevksi, Jian-Yu Cheng , and Georges L. Chahine
DYNAFLOW, Inc. 7210 Pindell School Road, Fulton, MD 20759
alexei@dynaflow-inc.com http://www.dynaflow-inc.com/

1. Introduction

The steepening of the forward face of waves and their subsequent breaking and overturning has been the focus of experimental and theoretical research for several decades. These waves are powerful agents responsible for water aeration, spray propagation in the atmosphere, and sediment transport. Breaking waves also affect the stability of offshore structures and the dynamics of ships and floating structures.

This work is part of an effort to simulate the influence of breaking waves on the motion of the next generation US Marines Advanced Amphibious Assault Vehicle (AAAV) as it traverses through the surf zone. In this paper we summarize our on-going efforts to describe wave dynamics as the waves advance over a constant slope beach. Experiments were performed in our wave tank with waves generated by a paddle wave maker, which can produce waves of varying amplitude and frequency. The geometry of the wave tank and the wave generation mechanism were modeled in both a 2D and a 3D numerical wave tank using DYNAFLOW's 2DWAVE and 3DYNAFS codes formulated from inviscid two and three-dimensional Boundary Element approaches.

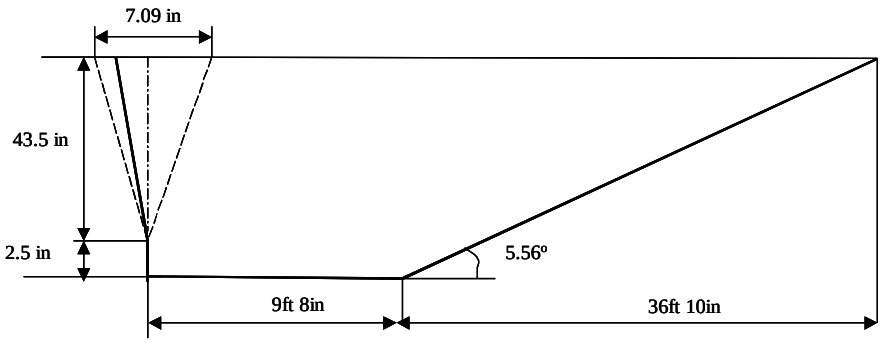

Fig.1. Experimental Setup in the DYNAFLOW Wave Tank.

2. Experimental setup

The experimental study was conducted in DYNAFLOW's 72 ft. long and 57 in. wide wave tank having a paddle wave maker 58 in. high and 56 in. wide at one end. The wave maker was hinged 2.5 in. above the bottom and situated 1 ft. away from the end wall of the wave tank. The wave maker frequency and stroke length were varied producing waves of frequency of 0.23Hz to 0.74Hz and wavelength of 110 in. to 550 in. The experiments were performed for both constant depth and sloping beach. The sloping beach was made of marine plywood installed at 10 ft. 8 in. from the end of the tank. Its angle could be varied. The results shown below are all for an angle of 5.56° (Fig.1). To measure wave height and wavelength we used two video cameras with fields of view of 3 ft. and 17 ft. We also utilized a capacitance-based probe for wave elevation measurements. The voltage from the probe was fed to GPIB interface card, and the data

were digitized and stored on a hard disk. The data were sampled at six locations: 20', 10', 6', 48", 33", and 20" far from the end of the beach. This enables characterization of the shape of the breaking waves as well as the time history of wave elevation.

3. Mathematical Formulation

It is widely accepted that the inception of wave breaking can be described in the framework of the potential theory [1-3]. We apply Green's identity to relate the potential at a field point P to the values of the potential and its normal derivative on the domain boundary S,

$$\alpha(P)\phi(P) = \int_S [G\left(\left|\vec{P}-\vec{M}\right|\right)\frac{\partial\phi}{\partial n}(M) - \frac{\partial G\left(\left|\vec{P}-\vec{M}\right|\right)}{\partial n}\phi(M)]ds, \qquad (1)$$

where a is a geometric coefficient, and G(x)=1/x in 3D or log(x) in 2D is the Green's function. To compute this integral numerically, the boundary S is discretized into triangular elements in 3D and linear elements in 2D [4,5]. We introduce double nodes at the corners of the fluid domain as in [6] and single nodes elsewhere. These corner nodes represent points where the free surface intersects the wave maker boundary and the sloping beach. We apply linear interpolation of the potential and its normal velocity resulting in a system of algebraic equations of the form:

$$\mathbf{B}\phi - \mathbf{A}\partial\phi/\partial n = 0, \qquad (2)$$

where **A** and **B** are matrices of rank N, and ϕ and $\partial\phi/\partial n$ are vectors of dimension N. On the free surface of equation $f(x,y,x,t)=0$, the potential ϕ satisfies the kinematics and dynamic boundary conditions:

$$df/dt = 0 \;|_{\text{on the FS, } f=0}, \qquad \partial\phi/\partial t + \left|\vec{\nabla}\phi\right|^2/2 + gz + \lambda\phi = 0, \qquad (3)$$

where l is a numerical damping factor which represents an artificial dissipation [7,8]. In computations this dissipation factor is described by a sinusoidal distribution with values varying from 0.003 (far from the beach) to 0.3 (at the end of the beach). The presence of this "sponge layer" allows dissipation of the energy as the wave approaches the beach.

On the wave tank bottom S_B and on the wave maker surface S_w a non-penetration boundary condition is written as,

$$\frac{\partial\phi}{\partial n}|_{S_B} = 0, \qquad \frac{\partial\phi}{\partial n}|_{S_W} = \dot{\theta}_W(t)\cdot r(t_0), \vec{r}(t) = r(t_0)\cdot\left(\hat{e}_r + \theta_W(t)\cdot\hat{e}_\varphi\right), \qquad (4)$$

where θ_W is the angular coordinate of the wave maker arm and $\hat{e}_r, \hat{e}_\phi$ are the unit vectors. Equations (2)-(4) form a closed system, that is solved using a time stepping procedure.

4. Experimental and numerical results

Four initial positions of the wave maker arm were considered: front, back or middle position where the arm could initially move backward or forward. The differences in the initial positions result in a phase shift of the generated waves. In what follows we report results related to the middle position of the wave maker moving initially forward. The wave maker arm stroke length was 10 inches and the frequency of its oscillation was 0.53 Hz. The displacement of the arm was measured and then approximated by a cubic spline-fit for the initial half period, and with a sinusoidal function fit thereafter. These data were used in the boundary conditions (4).

To enable the computation to continue beyond the breaking of the first wave and to simulate the behavior of the following waves, wave overturning must be suppressed. To achieve this objective we applied a "peeling" technique similar to that used in [2], where the top of the wave crest was peeled off when the height exceeded a critical value. Here, we employ a wave steepness criterion instead of the wave height – we prevent the wave slope from exceeding a critical value. The potential on the new surface is then obtained by applying a sliding window average to the values on the old surface. We used this approach in the 2D simulations only, the 3D simulations did not require it partly because of the coarser grids used. Figure 2 shows wave heights versus time at two locations in the numerical tank and illustrates the fact that the procedure allows the computations to proceed over long periods of time, while not significantly affecting the results in regions away from breaking. In the breaking region the maximum wave height values are affected while the overall behavior is little modified.

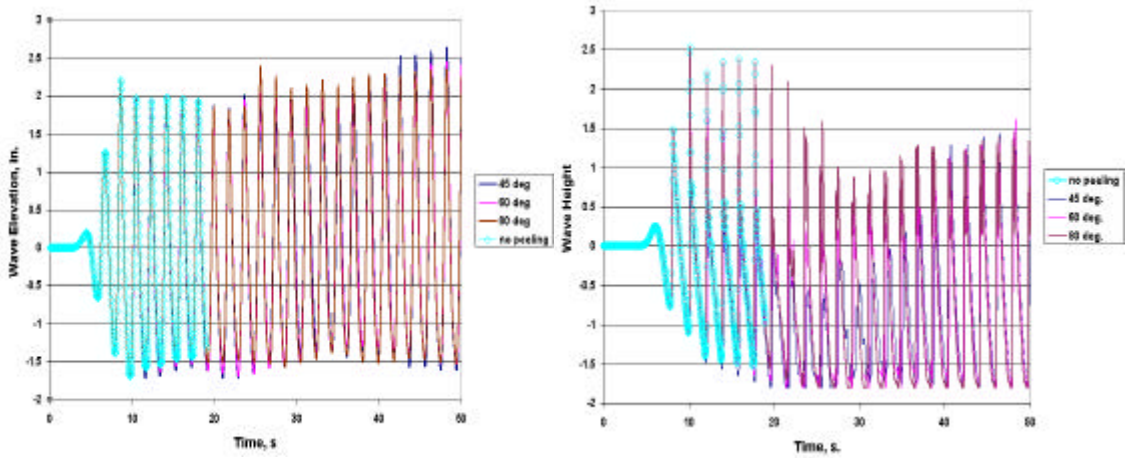

Fig. 2. Influence of the limit maximum steepness or local angle in the "peeling" technique on the wave height vs. time at two locations in the wave tank 10 ft. and 33 in. from the beach.

A convergence study was conducted for both time step size and grid size. This study showed that for the 2D 40 nodes per wavelength insured convergence, 17 nodes were enough in the 3D code [8]. The time-stepping scheme employs a variable step size proportional to the ratio of minimum grid spacing and maximum velocity. The convergence study determined the proportionality constant. The numerical solutions of 2D/3D codes were then compared to the experimental data obtained in a constant depth wave tank. Figure 3 illustrates amplification in the experiments of the wave amplitude at about 25 seconds, at 28 feet away from the wave maker. This is the time after which the waves reflecting from the end of the tank reach the observation point. In the experiments installing wave absorber at the end of the tank damped only partially these waves. Waves damping using the same parameters appear stronger in the 2D computations than in the 3D computations.

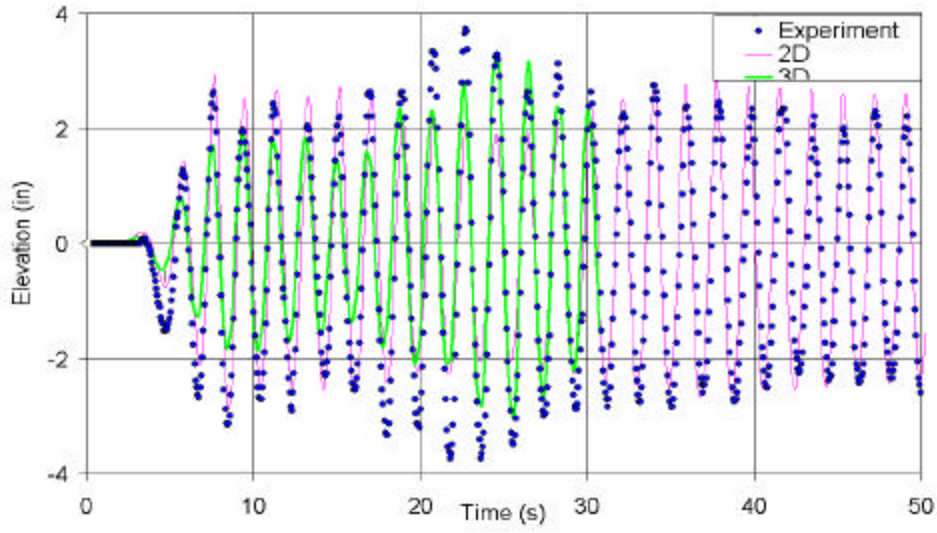

Fig. 3. Comparison of numerical results against experimental data for constant depth tank.

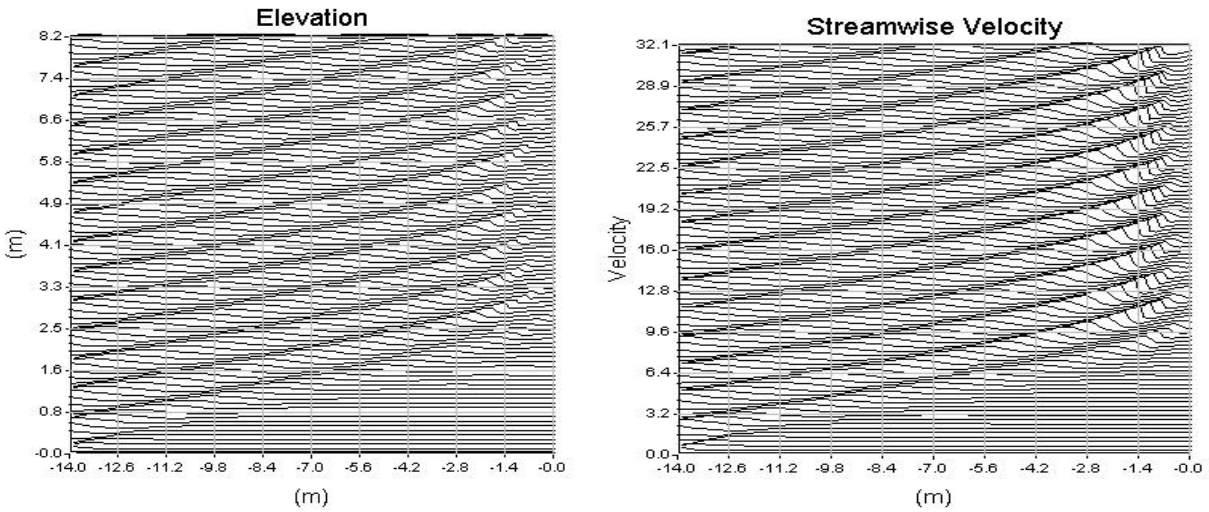

Fig. 4. Evolution of wave elevation and streamwise velocity in time.

Next, we studied wave performance on a slopping beach. A typical distribution of wave elevation and horizontal velocity distribution variation with time is shown in Fig. 4. Here the waves propagate from left to right toward the beach, and time grows along the y-axis. Fig.5 shows for the same test case the velocity distribution in the fluid domain at various computation times.

Fig. 6 shows wave elevation time history at 10 feet (left) and 33 inches (right) from the beach computed by both codes and compared against experimental data. While the fine details are different between the three, the overall character is very well captured by both the 2DWAVE and the 3DYNAFS codes even in the breaking region.

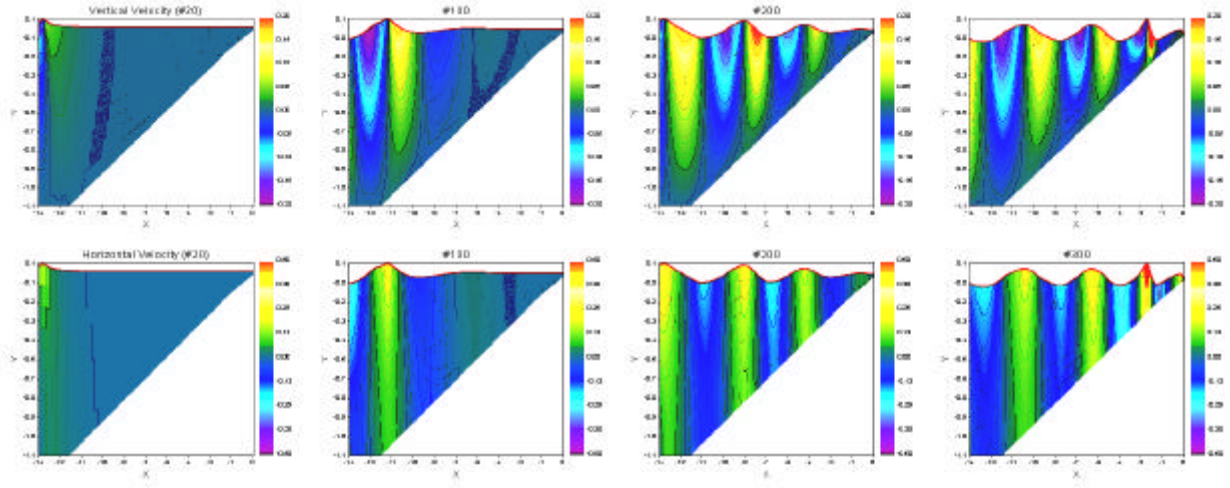

Fig. 5. Distributions of vertical (top) and horizontal (bottom) velocities in the fluid region.

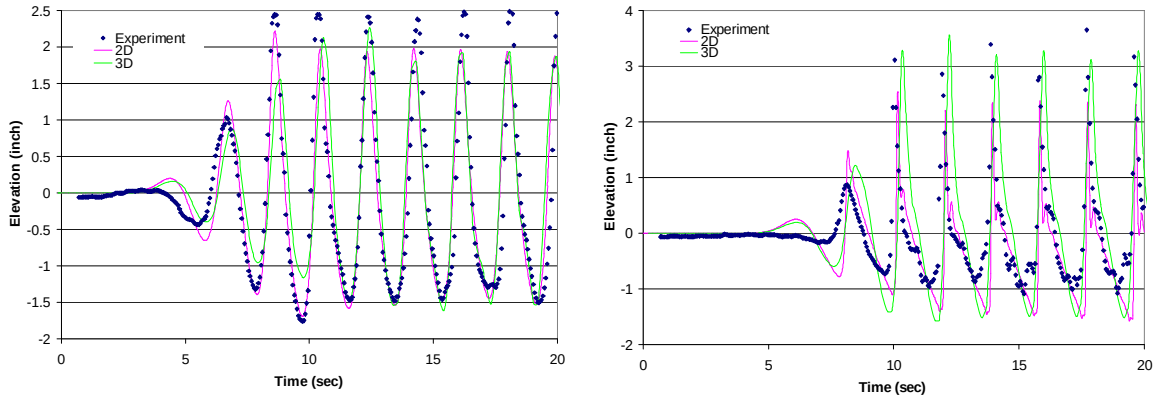

Fig. 6. Wave elevation vs. time at 10 ft. (left) and 33 in. (right) from end of sloping beach.

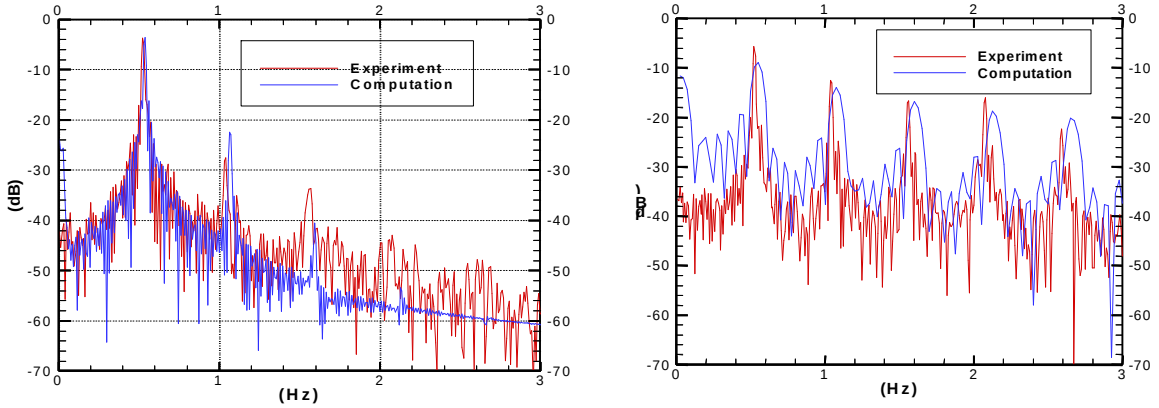

Fig. 7. Comparison of computed and experimental power spectra of wave elevation measured at distances of 20 feet (left) and 33 inches (right) far from the beach.

As the waves approach the beach the waves dynamics becomes highly nonlinear. Figure 7 presents power spectra of wave elevation both measured and computed at distances of 20 feet and 33 inches far from the beach. The spectra were normalized by the total power in each case. Farther from the beach the spectra exhibit a strong peak at the driving frequency of the wave maker while closer to the beach there are also several harmonics.

4. Conclusions

The time evolution of surface waves propagating over a shallow beach was simulated numerically with the aid of 2D and 3D Boundary Element codes. The waves were prevented from breaking by applying a "peeling" technique as well as by applying an artificial dissipating numerical beach. The numerical results show good overall agreement with the experimental observations. Wave steepening and nonlinear behavior close to breaking can be reasonably quantified using the developed numerical codes. Additional more detail work is still on-going in that direction.

Acknowledgments

This work was supported by Phase II US Marine Corps SBIR Contract, N61339-99-C-0060: *"High fidelity ocean surf zone model for use in USMC simulators"*.

References

1. Longuet-Higgins M.S. and Cohelet E.D., "The deformation of steep surface waves in water. I A numerical method of computation," Proc. R. Soc. London, Ser. A350, No. 1, pp. 1-26, 1976.
2. Wang P., Yao Y., and Tulin M. P., "An efficient numerical tank for non-linear water waves based on the multi-subdomain approach with BEM," International Journal for Numerical Methods in Fluids, Vol. 20, pp. 1315-1336, 1995.
3. Chen G. and Kharif C., "Two dimensional Navier-Stokes simulation of breaking waves," Physics of Fluids, Vol. 11, No. 1, pp. 121-133, 1999.
4. Chahine, G. L. and T.O. Perdue, Simulation of the Three-Dimensional Behavior of an Unsteady Large Bubble Near a Structure, in *Drops and Bubbles*, edited by T.G. Wang, A.I.P. Conference Proceedings, **197**:169-187, 1989.
5. Chahine, G., Duraswami, R, Kalumuck, K. (1997). Boundary Element Method for Calculating 2D and 3D Underwater Explosion Bubble Behavior Including Fluid Structure Interaction Effects," Naval Surface Warfare Ctr. Tech. Rpt. NSWCDD/TR-93/46.
6. Grilli S.T. and Svedsen I.A., "Corner problems and global accuracy in the boundary element solution of nonlinear wave flows," in Engineering Analysis with Boundary Elements, Vol. 7, No. 4, pp. 178-195, 1990.
7. Clement, A., Coupling of two absorbing boundary conditions for 2D time-domain simulations of free surface gravity waves, *J. Comp. Physics*, **126**: 139-151, 1996.
8. Cheng J-Y., Goumilevksi A., and Chahine G. L., "A 3D Boundary Element Method Simulation of Breaking Waves on a Gentle Beach," in EM2000.